Mine Water and the Environment (2022) 41:921–937
https://doi.org/10.1007/s10230-022-00909-z

TECHNICAL ARTICLE

Groundwater Source Identification and Flow Model of the Dareh-Zar Copper Mine in Central Iran by Chemo-isotopic Techniques

Sepideh Mali[1] · Hadi Jafari[1] · Reza Jahanshahi[2] · Rahim Bagheri[1]

Received: 20 January 2021 / Accepted: 30 October 2022 / Published online: 11 November 2022

Abstract

Seepage with AMD characteristics is observed in the Dareh-Zar copper mine in central Iran and more water inrush events are expected since the pit extends below the local groundwater levels. In order to properly design a dewatering system, it was necessary to determine the source of this groundwater and to establish a groundwater flow model. Thirty-nine water samples were collected from springs, qanats, observation wells, seepages, and permanent river water and analyzed for major ions, silica, Fe, Cu, and stable isotopes (^{18}O and ^{2}H). The electrical conductivity and pH of the water samples ranged from 403 to 4810 µS/cm and 3.3 to 8.6, respectively. The PCA and biplot diagrams confirmed the role of mineral weathering, redox reactions (Fe^{2+} release), and gypsum dissolution on groundwater chemistry outside of the pit and the effects of pyrite oxidation on weathering and dissolution reactions inside the pit. Based on hydraulic features inferred from the iso-potential map of the aquifer and cluster analysis of the chemical data, two distinct groundwater sources from the northwest and east of the mine, with fresh (Ca-HCO_3) and brackish (Na-SO_4) signatures, respectively, were identified as the possible sources of the Ca-SO_4 groundwater in the mine pit. The dramatic difference in Na concentrations in most of the samples does not support groundwater evolution to Ca-SO_4 types in the pit simply by mixing. Instead, the Ca-HCO_3 groundwaters from the north and northwest areas likely evolve to the Ca-SO_4 water-type in the pit due to pyrite oxidation. The stable isotopes indicated groundwater recharge zones at elevations ranging from 2479 to 2877 m above mean sea level, which is, on average, 207 m above the pit area and suggests that the north and northwest recharge zones are the primary source of the groundwater inrushes. These results are being used to help design a dewatering scheme for this mining area.

Keywords Acid Mine Drainage · Groundwater Invasion · Stable Isotope · Pyrite Oxidation

Introduction

Ores, minerals, and aggregates are often extracted via open pits. In some cases, the pits extend below the local groundwater levels, which can make the pit vulnerable to groundwater inrushes that can cause operational and technical problems such as pit wall instability, inefficient excavation and haulage, reduced production efficiency, and increased maintenance costs (Heidari-Nejad et al. 2017), as well as environmental concerns (Jahanshahi and Zare 2015). Sometimes, large volumes of water flow into the mine under high pressure, which can be disastrous (Gu et al. 2018). Hence, mine water disaster management and prevention are very important (Xu et al. 2018). Prediction and prevention of water inrush have been extensively studied (e.g. Guo et al. 2018; Hu et al. 2014; Hu et al. 2019a, b; Lee et al. 2013; Li and Wu 2019; Li et al. 2018; Wu et al. 2016, 2017; Zhang and Yao 2020; Zhao et al. 2013; Zhou et al. 2018a, b).

Dewatering systems are usually designed to drain the mining front by diverting groundwater flow from the pit area (Struzina et al. 2011). The success of a drainage scheme mainly depends on identifying the source of the groundwater seeping into the pit (Qian et al. 2018). Many methods have been developed to determine the groundwater origin, among which hydrochemical and isotopic techniques are widely used (e.g. Heidari-Nejad et al. 2017; Jahanshahi and Zare 2017; Qian et al. 2018; Xu et al. 2018; Yang et al. 2020). Hydrogeological methods, such as pumping tests and injections, can be costly and inefficient, so hydrochemical

✉ Hadi Jafari
h_jafari@shahroodut.ac.ir

[1] Faculty of Earth Sciences, Shahrood University of Technology, Shahrood, Iran

[2] Department of Geology, Faculty of Science, University of Sistan and Baluchestan, Zahedan, Iran

approaches can be used to understand the evolution of groundwater (Gu et al. 2018; Li et al. 2016). Water quality and isotopic data can be used to distinguish water inflow sources with approaches such as multivariate statistics (Wu et al. 2014). The groundwater's chemical variations can help discriminate groundwater inrush sources (Huang et al. 2018). In combination with other data, isotopes, hydrology, and geology can be useful in understanding the characteristics of groundwater recharge and discharge areas (Gomo and Vermeulen 2014; Huang et al. 2018). However, mining activities can influence the geochemistry of groundwater and hydraulic connections, which may considerably reduce the accurate discrimination of inrush sources (Zhang et al. 2020). Stable isotopes can be used to help recognize the sources of water inrush, while mixing models can be used to infer the mixing ratios of the various groundwater types (Guan et al. 2019; Huang et al. 2019; Jin et al. 2018; Rambabu et al. 2018; Tomonaga et al. 2016; Zhang et al. 2020).

To sum up, analysis of the groundwater salinity in combination with ionic ratios and conventional hydrochemistry graphs (e.g. Stiff and Piper diagrams) are useful tools to classify water samples and differentiate groundwater origins (Amajor and Gbadebo 1992; Askari Malekabad et al. 2020; Faye et al. 2005; Ghiglieri et al. 2012; Jahanshahi and Zare 2017; Mondal et al. 2011; Yidana and Yidana 2010). In this regard, multivariate statistical analyses (e.g. principal components and cluster analysis) are commonly used to identify the influential factors in chemical compositions and to determine groundwater origins in mine pit areas (Ahmadi et al. 2018; Askari Malekabad et al. 2020; Ma et al. 2014; Shrestha and Kazama 2007; Wu et al. 2014; Wunderlin et al. 2001; Zhao et al. 2011).

Stable isotopes of water (^{2}H and ^{18}O) provide robust insight in groundwater source identification studies, as they change due to natural variations in precipitation, evaporation, and mixing of different waters (Sprenger et al. 2014). They are mostly applied to differentiate local and regional meteoric sources of the groundwater (Bahadori et al. 2019; Heidari-Nejad et al. 2017; Jurado et al. 2013). Without significant evaporation and mineral dissolution, the isotopic compositions of the groundwater are the same as the precipitation, lying on the local meteoric water line (LMWL; Clark and Fritz 1997). Stable isotopes have been used in many studies to assess groundwater origin (e.g. Ahmadi et al. 2018; Alegbe et al. 2019; Askari Malekabad et al. 2020; Bahadori et al. 2019; Cao et al. 2019; Christensen et al. 2018; Gamboa et al. 2019; Gomo 2018; Hao et al. 2019; Jahanshahi and Zare 2017; Jamal 1991; Karolytė et al. 2017; Larkins et al. 2018; Lenter et al. 2002; Naderi et al. 2020; Pyrbot et al. 2019; Sahraei Parizi and Samani 2013; Sahraei Parizi and Samani 2014; Shojaei Baghini et al. 2020; Skousen et al. 2019; Tomiyama et al. 2019; Yolcubal et al. 2017; Zhou et al. 2018a, b), especially in source identification of groundwater in mining areas threatened by groundwater invasion (e.g. Ahmadi et al. 2018; Heidari-Nejad et al. 2017; Jahanshahi and Zare 2017; Ma et al. 2016; Qian et al. 2018; Sahraei Parizi and Samani 2014; Xu et al. 2018; Yang et al. 2021).

After recognition of various water sources (end members) in the mining pit area on a hydrochemical and isotopic basis, mixing models based on water and mass salt balance (Scheiber et al. 2018) can help to assess mixing ratios and quantify relations between different groundwater sources (Pitkänen et al. 1999). There are always uncertainties involved in the assessment of end-member contents and evaluation of mixing ratios, so Carrera et al. (2004) developed a method of multivariate statistical analysis to perform calculations of mixing ratios while acknowledging the uncertainties of end-member compositions.

The Dareh-Zar copper mine is in the initial stages of operation and excavations have created a mining pit with an average surface area of about 1.5 km^2 and a depth of 120 m. The base of the pit is now 2526 m a.m.s.l. (m above mean sea level), below the mean groundwater level of the local aquifer (2650 m a.m.s.l.) Many seepage faces with acid mine drainage (AMD) characteristics are currently observed in the pit, and more groundwater incursions are expected as the pit grows deeper. Since the dewatering system of the mine pit is still being designed, more information on the groundwater system was needed, especially regarding the probable sources of groundwater in the pit area. Hence, this study was undertaken, to identify groundwater sources in the Dareh-Zar mining area using chemical and isotopic techniques and to model groundwater inrush into the pit. The factors that control the chemo-isotopic signatures of the groundwater were determined and a hydrogeological model explaining the chemistry and the origin of the groundwater seeps in the pit was developed. The results will be used to design the dewatering scheme in this area.

Materials and Methods

Site Description

The Dareh-Zar porphyry copper deposit is in Kerman province in central Iran, about 10 km south of the better known Sarcheshmeh copper mine, at geographic coordinates of 55°53' N and 29°52' E; both mines are located on NW–SE trending mineralization zone of Band-e-Mamezar (Fig. 1). The geology of the study area is complex due to multi-phase magmatic intrusions, as well as the effects of alteration and tectonic structures. Andesitic-basalt lava flows of the Eocene age with fine-granular porphyry texture are the major rock units hosting the porphyry copper deposits. From a tectonic

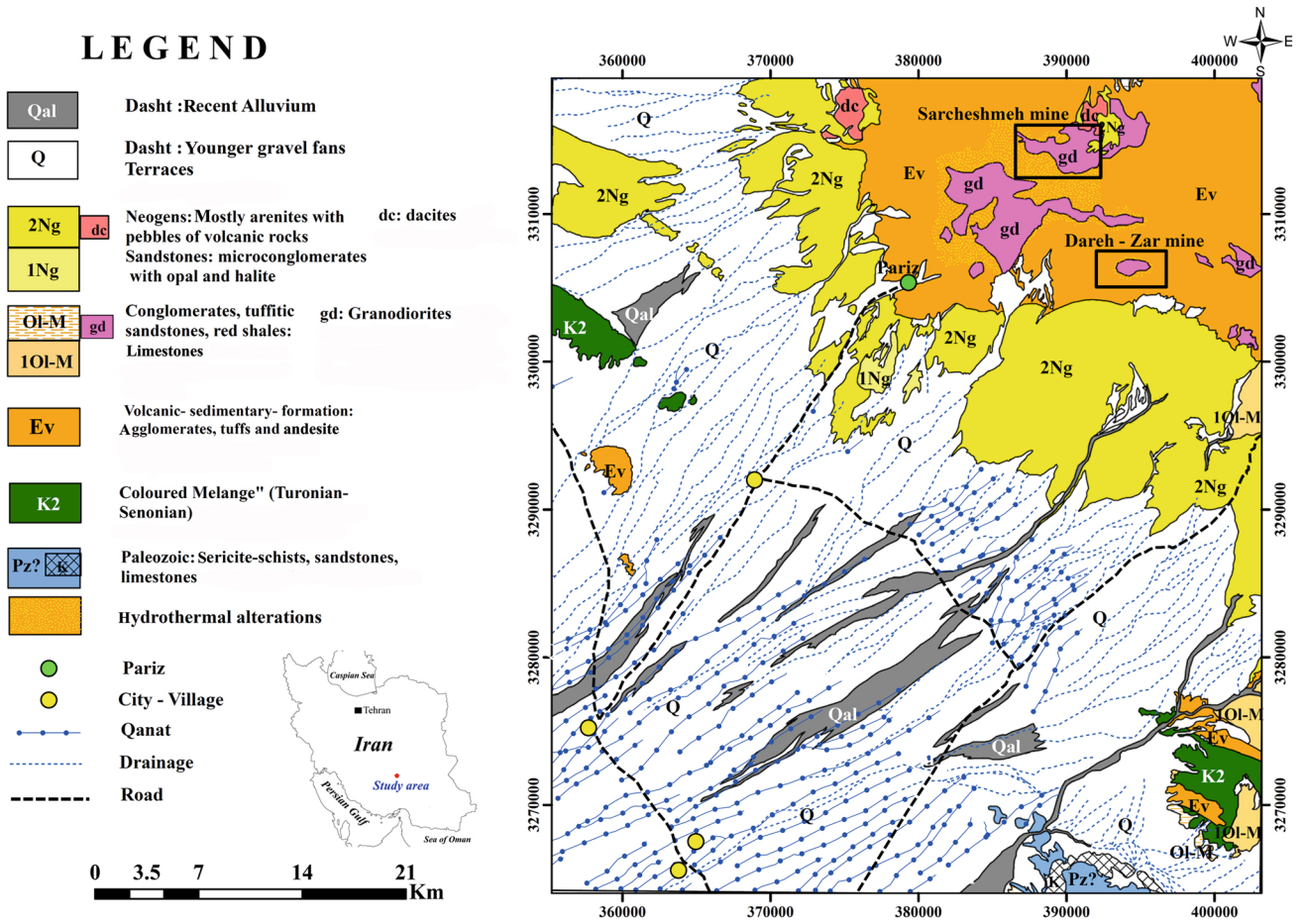

Fig. 1 Geological map of the Dareh-Zar and Sharcheshmeh copper mines, adopted with minor corrections from 1:100,000 geological map of Pariz (Dimitrijevic et al. 1956)

viewpoint, the area is affected by two major N-S and E-W fault systems accompanied by some secondary fracturing structures. In the upper parts of the copper deposit, the downwash process has expanded and caused secondary enrichment in the lower parts. In most areas of the downwash area, primary sulphides have been replaced by iron oxides and hydroxides; the copper grade is in the range of tens to several hundred grams per ton. In the deposit area, phyllic, propylitic, and argillic alteration zones are observed, and the potash alteration has a limited outcrop. Phyllite alteration is widespread in the study area and includes quartz, sericite, and pyrite. Propylitic alteration occurs in the marginal parts of the deposit and in the volcanic units and dikes. The copper ore of the mine has a porphyry texture and includes plagioclase, amphibole, quartz, and biotite macro-crystals. In these rocks, most amorphous and large plagioclase and amphibole crystals are in a matrix of alkaline feldspar and fine quartz crystals. The ferromagnesian minerals in this ore mass are amphibole and biotite. In some rock samples, secondary minerals of epidote and chlorite are also observed.

In the study area, secondary porosity and permeability due to weathering and fracturing has created a hard-rock double-porosity aquifer. Therefore, the hydraulic properties of the aquifer are mainly controlled by fractures. The hard rock aquifer generally represents heterogeneous and anisotropic media (Mali et al. 2021). Groundwater is being discharged at a few springs, qanats, and seeps. A qanat (or kariz) is a system that transports water from an aquifer to the surface through an underground aqueduct. A qanat is constructed as a series of well-like vertical shafts connected by a gently sloping tunnel and taps underground water and delivers it to the surface by gravity, without pumping. Fifteen observation wells, named as DW (vertical wells) and GDZ (diagonal wells) were installed in the mine area (Fig. 2A) to monitor the groundwater levels. Based on the iso-potential map of the aquifer (Fig. 2A), groundwater is generally flowing from the northwest to the southeast. Curvature in equipotential lines is observed due to the pit excavations and related dewatering processes. Furthermore, concentrated discharge of the

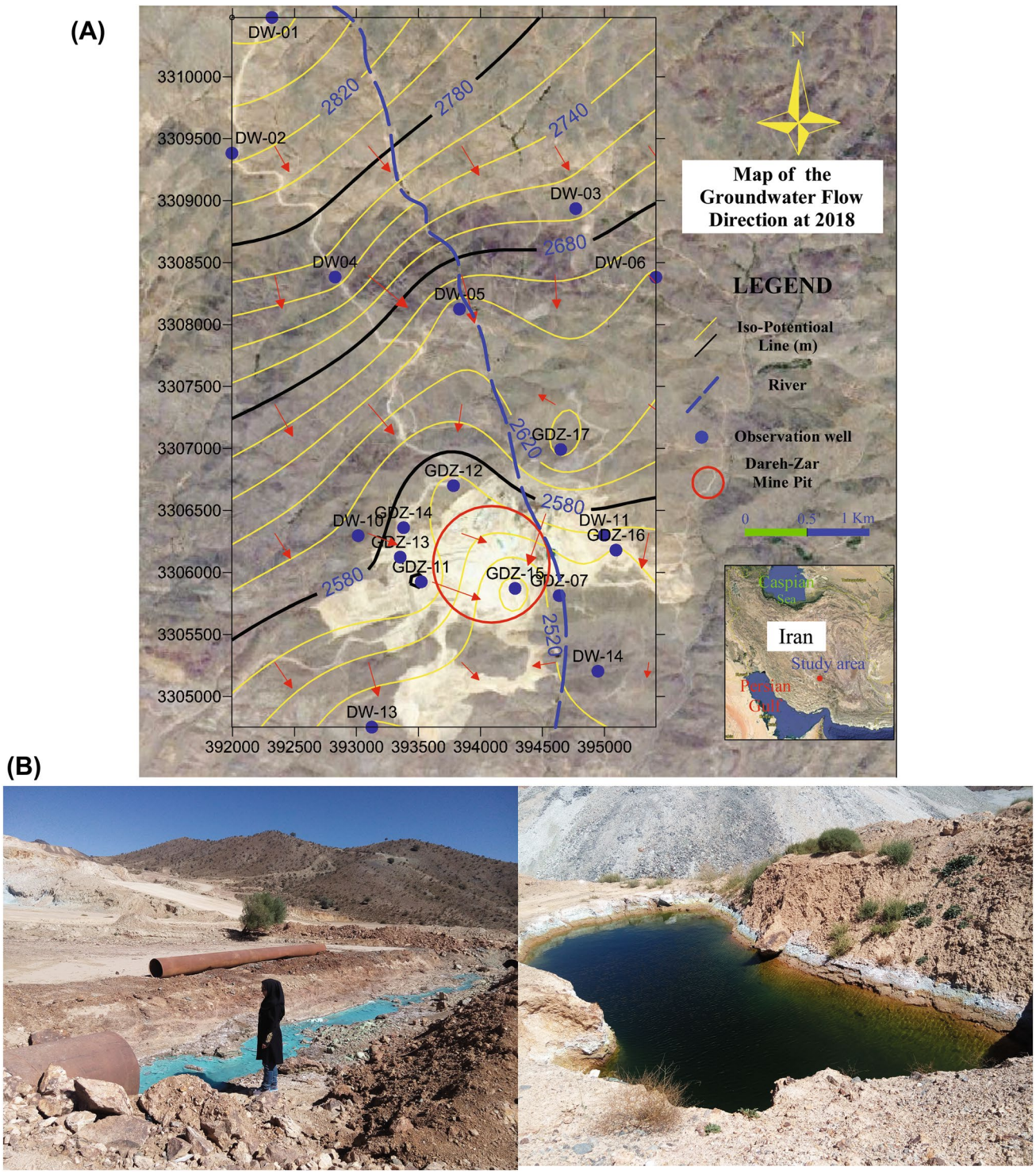

Fig. 2 Iso-potential map and groundwater flow direction in the Dareh-Zar mine (**A**) and formation of seepages with acid mine drainage (AMD) characteristics in the pit (**B**)

groundwater through the pit area causes a cone of depression to develop, enhancing groundwater inrush into the mine and related problems such as flooding, instability of the pit walls, and AMD production (Fig. 2B). In a similar trend to the groundwater flow direction, a permanent river is flowing in the study area that finally drains the aquifer toward the south. Changes in the water table in this area are mainly affected by fluctuations in precipitation and river discharge. The most water table fluctuations were observed in well DW1 (Fig. 2A; Mali et al. 2021).

Sampling and Analysis

Water resources were sampled both in the wet and dry seasons. Since wet season samplings were more complete and better distributed, only the data for the wet season were examined in this research. In total, 39 water samples (Fig. 3A) were collected from observation wells, seepages, spring, qanats, and the river in June 2018 and analysed.

Temperature, electrical conductivity (EC), pH, and Eh of the water samples were measured in-situ using a portable Hanna multi-range EC meter-HI8733 and AZ pH meter-8601, respectively. To separate the suspended particles, water samples were filtered in-situ by a 0.45 µm syringe filter and then moved to clean polyethylene bottles. The bottles for major cation analysis were treated with HNO_3 (65%) to guarantee their dissolution. The concentrations of major cations (Ca, Mg, Na, K), Cu, Fe, and Si (converted to SiO_2 by mass balance approach) were measured using an ICP-MS device (HP Agilent 4500), Cl, and HCO_3 were measured using the titration method, and SO_4 was measured by spectrophotometry (turbidimetry method) in the Iranian Zarazma Laboratory. The ion balance (IB) error was calculated:

$$IB = \frac{\left|\sum Anions(epm) - \sum Cations(epm)\right|}{\sum Anions(epm) + \sum Cations(epm)} \quad (1)$$

The analytical results are presented in Table 1. Except for the low pH water sample, all analyses had an IB < 5%.

The 60 mL grab samples were collected in dark bottles to be analyzed for ^{18}O and ^{2}H in the Stable Isotope Laboratory of the Atomic Energy Agency of Iran. The results are reported in ‰ relative to the Vienna standard mean ocean water (VSMOW) standard with a precision of ± 0.6 ‰ (2σ) and ± 0.1‰ (2σ) for δ^2H and $\delta^{18}O$, respectively (Table 1). The limits of instrumental detection, accuracy, and precision of the data analysis (QC/QA measures) are provided in Table 2.

Saturation indices (SI) with respect to calcite, dolomite, gypsum, halite, Cu-and Fe-bearing minerals such as chalcopyrite, azurite, ferrohydrite, langite, malachite, nantokite, tenorite, Cu-metal, hematite, and pyrite were calculated using the PHREEQC software (Parkhurst and Appelo 1999).

Hierarchical cluster analysis (HCA) and principal components analysis (PCA) were used to determine the relationship between physicochemical parameters in the water samples. PCA is used to reduce complex and numerous datasets into a smaller number of components while maintaining the information content (Qian et al. 2016; Zhang et al. 2020). HCA can be used to classify water samples by their hydrochemical indicators (Liu et al. 2019; Zhang et al. 2020). Statistical analyses were performed using XLSTAT software, which allows users to analyse results with Microsoft Excel.

The probable origin of the groundwater in the Dareh-Zar pit area was investigated using a mixing model at the local scale, considering the composition of end-members and their percentage in the pit waters. The calculations were performed using MIX PROGRAM v1.0 (Carrera et al. 2004), which evaluates mixing ratios in the case of uncertain endmembers. The code is constructed based on the method of maximum likelihood to obtain the mixing ratios (Scheiber et al. 2018).

Results and Discussion

Hydrochemistry of the Mine Waters

The electrical conductivity (EC) of the groundwater in the study area ranged from 403 to 4810 µS/cm (Table 1). The lowest EC was recorded in well DW1 in the northwest portion of the mine and the highest was observed in artesian piezometer DW7 in the east. In a similar trend to the EC, the groundwater salinity increases to the east and centre of the mine. The pH of the water samples ranged from 3.26 to 8.62, showing neutral-alkaline and acidic features outside and inside the pit, respectively. The Eh of the groundwater ranged from -108 to 229 mv. The spatiality of the data confirmed a generally reduced state outside of the pit (negative to 0 Eh), and oxidizing conditions inside the pit (positive Eh). Spatial distribution of SO_4 and Cl show that SO_4 increases to the centre of the mine while no trends were observed in Cl content. Regarding the lithology, which mainly consists of igneous rocks, groundwater alkalinity increases due to dissolution of carbonate minerals. This explains the dominant groundwater type (Ca-HCO_3) in most samples as observed in the Stiff diagrams (Fig. 3A). Toward the mining pit, the type of water changes to Ca-SO_4 due to oxidation of S-bearing minerals in the mine area. The water type in the brackish water sample of DW7 is Na-SO_4, probably due to alteration of Na-plagioclase and oxidation of S-bearing minerals. The geological map (Fig. 1) and research by Sahraei Parizi and Samani (2013, 2014) and Khorasanipour and Eslami (2014) show that the agglomerates, andesite, and tuffs generally contain large amounts

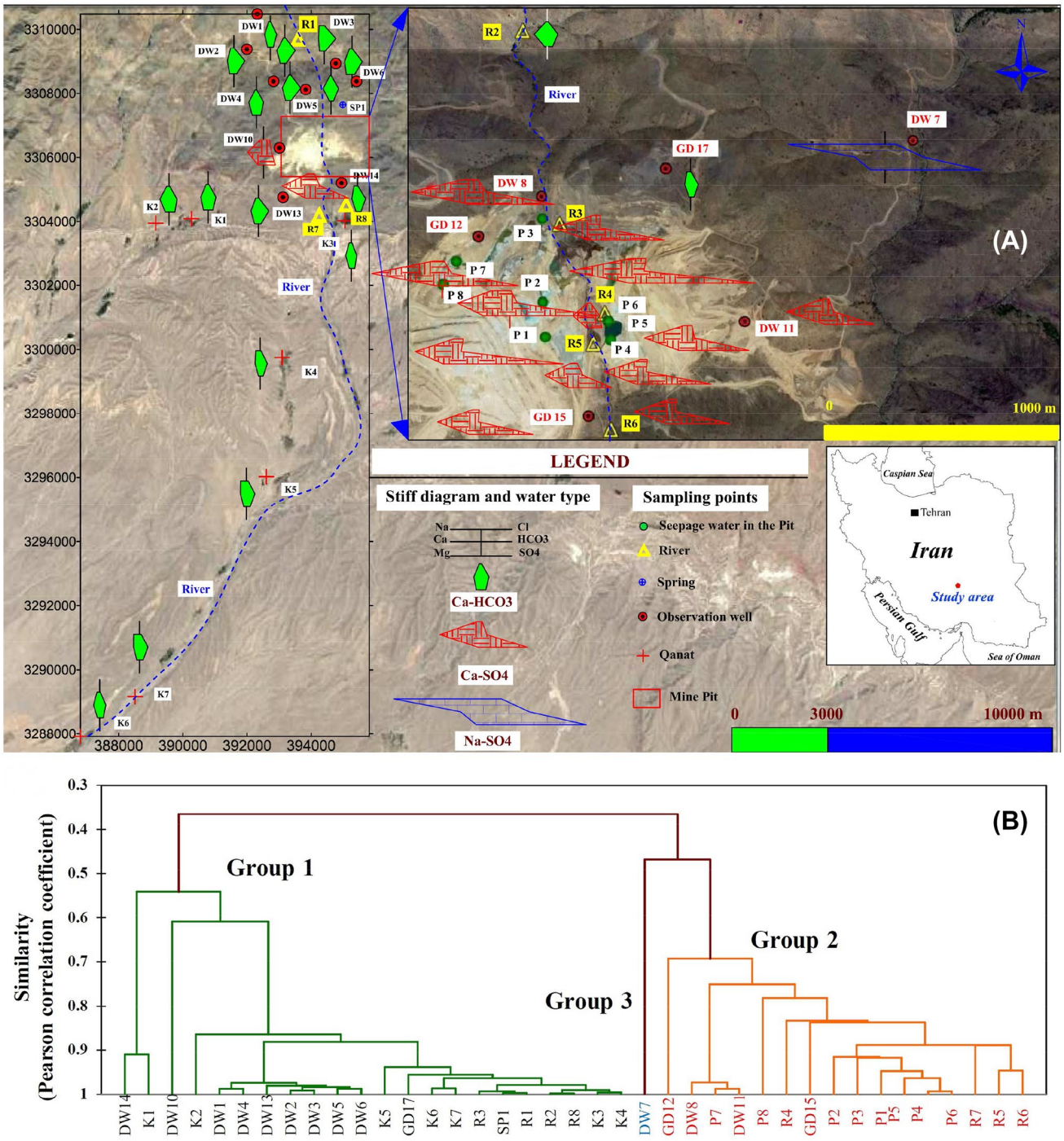

Fig. 3 The location map of the water samples and spatial distribution of water types based on Stiff diagrams in the study area (**A**) and clustering the water samples into three groups on a dendrogram (**B**)

of sodium plagioclase and andesine (Williams et al. 1982), which is widely spread in the study area. On the other hand, well logging at DW7 location shows a highly weathered and crushed 12 m thick layer of andesite. This weathered layer is also detected at levels above the water table elevation in other wells. Therefore, release of Na from the weathering process is the probable source of Na in this sample. Evaporite sediments containing halite (NaCl), gypsum ($CaSO_4$), and mirabilite (Na_2SO_4) that outcrop in the region (Fig. 1) are the other possible source of Na-SO_4 water in the study area.

Table 1 Physicochemical properties of the water resources in the study area: EC (μS/cm), Eh (mv), temperature (°C), major ions, minor elements and SiO_2 (mg/L) and stable isotope of $\delta^{18}O$ and $\delta^{2}H$ (‰ VSMOW)

Place	Name	EC	pH	Eh	T	Na	K	Ca	Mg	Cl	SO_4	HCO_3	Cu	Fe	SiO_2	$\delta^{18}O$	$\delta^{2}H$
Spring	SP	474	8.32	− 108	27	12.1	0.51	80	8.9	5.8	62	237.9	32.20	0.16	7.80	− 6.36	− 29.07
Seepage in the pit	P1	2497	3.26	229	19.1	58	5	328	78.7	27	1740	0	70.31	17.64	33.90	− 5.24	− 31.28
	P2	1945	3.35	223	20.2	42	6.5	92.7	64.4	16	1250	0	89,200	16.00	10.43	− 4.29	− 22.38
	P3	2524	6.47	39	26.3	110	8.5	531	59.5	27	1900	0	0.51	0.12	16.65	− 3.34	− 22.31
	P4	1438	4.30	166	18.9	46	6	300	42.8	14	1111	0	23.15	2.35	16.48	− 3.34	− 23.93
	P5	1618	4.61	148	18	50	5	328	49	19	1000	91	2598.30	0.03	11.74	− 3.26	− 23.8
	P6	1664	4.63	147	18.9	45.9	6	328	48	13	1111	0	23.73	1.44	16.91	− 3.32	− 23.1
	P7	2310	7.40	− 18	21.3	70	7	503	28	23	1300	205	0.01	0.04	19.08	− 6.37	− 37.39
	P8	2049	6.69	24	20	140	19	373	115	13	1500	162	4.57	0.03	24.94	− 5.19	− 32
Piezometer	DW1	403	8.62	− 87	16.2	9	1	66.36	22.4	2	10	320	0.23	0.00	5.23	− 5.72	− 30.74
	DW2	522	7.83	− 40	15.6	47	2	62.6	26.9	2	8	448	2.00	0.03	6.39	− 6.7	− 38.27
	DW3	509	7.31	143	25	68	2.5	45.7	31.1	9	33	420	0.02	0.05	8.34	− 6.26	− 37.99
	DW4	528	7.63	− 32	16.1	15	2	96.5	28.4	12	156	261	0.90	0.02	5.27	− 6.61	− 38.33
	DW5	638	7.94	− 49	17.5	15	3	96.4	29.8	17	48	392	103.20	0.10	9.11	− 5.95	− 34.01
	DW6	544	7.67	− 33	19.7	27	2	88.8	36.5	15	65	462	4.00	0.08	6.19	− 6.72	− 32.86
	DW7	4810	7.67	− 34	22.6	1284	25	140	104	248	2950	191	0.02	7.82	4.50	− 6.86	− 36.13
	DW8	2061	7.59	− 28	21.6	116	7	471	28.8	15	1328	189	0.03	0.16	18.68	− 6.14	− 35.78
	DW10	1020	7.58	− 28	18.1	36	3	193.5	36.1	102	372	220	0.03	0.50	9.32	− 6.69	− 36.54
	DW11	1951	7.25	− 8	20	59	5	518	23.6	11	1300	198	0.01	7.66	19.00	− 6.92	− 37.71
	DW13	650	7.50	− 24	19.7	32	3	74.2	22.2	14	78	327	59.30	0.80	11.00	− 6.01	− 35.1
	DW14	1205	7.71	− 35	20.6	249	12	88.9	51.4	71	300	691	0.01	0.06	11.64	− 6.01	− 35.67
	GD12	988	7.12	0	18.5	60	4	130.5	34.6	9	507	86	621.41	1.30	13.27	− 7.63	− 35.64
	GD15	2540	4.87	133	19.9	113	10	439	130	34	1976	0	165.39	49.91	18.09	− 8.07	− 38.49
	GD17	524	7.63	− 29	19.4	46	2	58.4	8.7	9	100	217	0.04	0.05	8.74	− 6.04	− 33.63
Qanat	K1	594	7.61	101	25	29	2	87.8	30.8	21	148	273	0.01	0.05	13.04	− 4.83	− 27.36
	K2	719	7.95	− 50	15.8	22	1.5	113.3	22.2	32	184	237	0.02	0.02	7.01	− 5.46	− 34.83
	K3	414	8.14	− 62	14.5	9	1	69.9	10.9	11	61	194	0.02	0.10	11.98	− 4.63	− 28.94
	K4	668	7.89	− 45	14	16	1.5	104.5	19.2	15	186	207	0.01	0.02	11.14	− 4.64	− 26.58
	K5	806	8.17	− 63	18.6	73	3	70.3	15.8	49	143	221	0.01	0.01	16.19	− 5.16	− 26.72
	K6	548	7.90	− 48	19.1	31	3	65.7	12.5	17	109	180	0.020	0.01	11.48	− 3.37	− 22.32
	K7	590	8.02	− 54	19	36	4	67.1	14.6	17	120	202	0.01	0.03	16.99	− 4.55	− 24.82
River	R1	445	8.11	− 57	20.2	10	1	92	11.2	12	90	232	0.01	0.04	8.39	− 4.59	− 27.32
	R2	527	7.90	− 48	15	7	1	81.2	11.3	12	120	169	0.01	0.04	7.83	− 5.29	− 30.07
	R3	643	7.92	− 48	15.5	16	1.5	120	14	13	206	211	0.01	0.03	9.58	− 5	− 28.54
	R4	1239	7.72	− 34	22.3	39	5	221	32.4	14	609	149	1842.40	0.02	12.56	− 5.55	− 22.6
	R5	1504	7.15	− 3	18.2	42	6	290	39.6	12	935	0	3.1	0.03	14.60	− 5.08	− 30.22
	R6	164	8.07	− 55	22.6	44	7	317	50	13	1000	58	0.34	0.03	15.59	− 4.05	− 25.45
	R7	1634	7.47	− 19	17.2	30	4	269	58	18	914	2	0.02	0.07	15.21	− 4.04	− 24.8
	R8	505	7.86	− 43	16.8	10	1	75.5	11.5	14	96	171	0.01	0.04	9.63	− 4.65	− 27.53

Hierarchical Cluster and Principal Component Analysis

Based on a dendrogram (Fig. 3B) derived from cluster analysis (HCA), the water samples were classified into three groups:

Group 1: Samples located outside the pit with Ca-HCO_3 water-type.

Group 2: Samples collected from inside the pit and nearby areas with dominant Ca-SO_4 feature.

Group 3: Brackish water sampled from piezometer DW7 with Na-SO_4 characteristic.

According to Khorasanipour and Eslami (2014), the Na-SO_4 water type is observed in surface waters from the tailings ponds of the Sarcheshmeh mine north of Dareh-Zar. In fact, Na_2S and/or NaHS compounds are used in the

Table 2 Limits of detection, accuracy error and precision of water samples analysis

Elements	Unit	Detection Limit	Accuracy error (%)	Precision* (% RPD)
HCO3	mg $L.^{-1}$	0.1	1	4.4
Cl	mg $L.^{-1}$	0.1	2	6.5
SO4	mg $L.^{-1}$	0.1	1	3.2
Ca	mg $L.^{-1}$	0.1	3	8.5
K	mg $L.^{-1}$	0.1	1	1.7
Mg	mg $L.^{-1}$	0.1	3	9.2
Na	mg $L.^{-1}$	0.1	1	7.5
Si	mg $L.^{-1}$	0.1	2	6.3
Cu	µg $L.^{-1}$	0.1	2.7	3.4
Fe	µg $L.^{-1}$	10	3.1	12.3
δ18O	%VSMOW	0.01	0.1	0.1
δ2H	%VSMOW	0.01	0.1	0.06

*The precision was calculated as %RPD (relative percent difference) by the following formula: %RPD = [abs (SV–DV) / 0.5 × (SV + DV)] × 100, where SV was the value of the original sample and DV was the value of the duplicate sample

treatment of copper ores, which means that sodium and sulphate can be released into the groundwater when the tailing storage facility is not lined or if there are leaks from the plant. This suggests that the groundwater chemistry of sample point DW7 could be due to the nearby Sarcheshmeh tailings ponds. However, this idea is not supported by the hydrogeological setting based on the following reasons:

1- The average height of the water table in the area of Sarcheshmeh mine is lower than the groundwater levels in the Dareh-Zar mining area (Fig. 4A). In addition, high drawdowns in the groundwater table are observed in the Sarcheshmeh pit area (Sahraei Parizi and Samani 2013), which would limit groundwater movement to the south, i.e. Dareh-Zar mine (Fig. 4B). In other word, groundwater movement from Sarcheshmeh to Dareh-Zar mine is not hydraulically possible.

2- The Sarcheshmeh tailing dams are about 30 km far from the Dareh-Zar mine, and the Sarcheshmeh pit is located midway, 19 km from Dareh-Zar (Khorasanipour and Eslami 2014). The groundwater flow direction in the Sarcheshmeh area is from the tailing dams toward the pit (Sahraei Parizi and Samani 2013), and therefore, the Na-SO_4 water type would first be observed in the Sarcheshmeh pit if leakage has occurred, and no Na-SO_4 water has been reported from the area (Sahraei Parizi and Samani 2014). This may be due

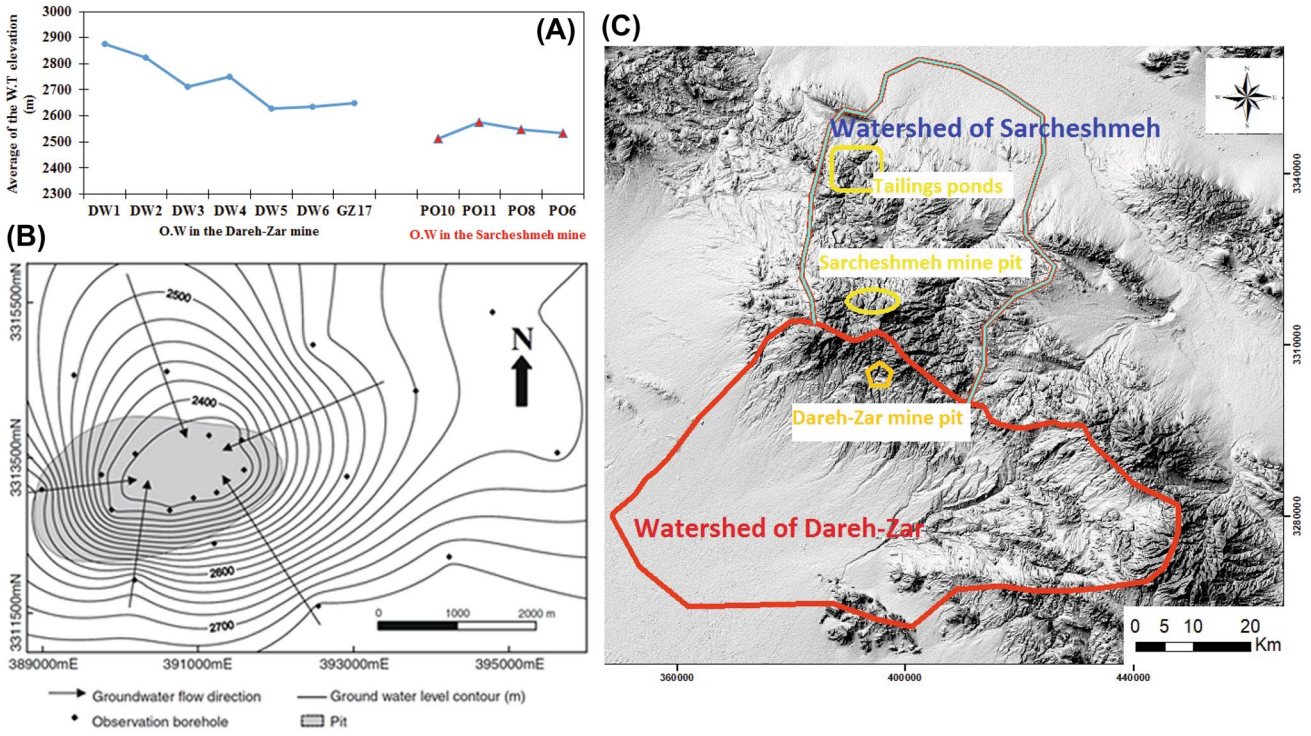

Fig. 4 Comparison of water table elevation in Sarcheshmeh and Dareh-Zar mines (**A**), groundwater iso-potential map in the Sarcheshmeh copper mine area (Sahraei Parizi and Samani 2013) (**B**), and the surface watersheds (basins) of the Sarcheshmeh and Dareh-Zar mining areas (**C**)

to the very low permeability of the 75 m thick bed of fine-grained sediments at the bottom of the tailings reservoirs (Khorasanipour and Eslami 2014), which limits wastewater infiltration into the underlying aquifer.

3- Surface topography and streams directions confirm that Sarcheshmeh and Dareh-Zar mines are located in separate hydrological basins (Fig. 4C).

Based on the cluster analysis, water resources were divided into two groups "outside the pit" (group 1) and "inside the pit" (group 2). Principal component analysis (PCA) was performed separately for the samples collected from "outside the pit", considering pH, Eh, EC, major ions, SiO_2, Fe, and Cu parameters. Based on the results, three major factors were identified for the samples from inside and outside the pit that totally explain 62.4 and 65.8% of the overall variance, respectively (Table 3).

Table 3 Component loadings on each variables using principal component analysis for water samples from inside and outside the pit. Bold values correspond to highest loadings

	Outside the pit (group 1)			Inside the pit (group 2)	
Variable	F1	F2	F3	F1	F2
pH	− 0.587	− 0.320	0.259	**− 0.830**	0.360
Eh	0.358	0.097	− 0.468	**0.832**	− 0.363
Na	**0.806**	− 0.161	− 0.272	0.212	**0.880**
K	**0.834**	− 0.184	− 0.189	0.126	**0.718**
Ca	0.396	− 0.097	**0.779**	0.015	**0.789**
Mg	**0.817**	− 0.315	− 0.235	**0.654**	0.433
Cl	0.772	− 0.125	**0.536**	**0.711**	0.382
SO_4	0.684	− 0.075	**0.650**	**0.721**	**0.611**
HCO_3	**0.649**	− 0.249	− 0.591	**− 0.535**	0.437
SiO_2	− 0.012	− 0.076	0.193	**0.539**	0.206
Fe	0.101	**0.931**	− 0.015	**0.865**	0.116
Cu	0.027	0.224	− 0.251	**0.714**	− 0.421
Eigenvalue	4.362	3.646	2.520	6.559	3.429
Variability (%)	27.262	22.790	15.750	40.992	21.430
Cumulative %	27.262	50.053	65.804	40.992	62.422

For water samples from outside the pit (group 1), the first principal component (F1) explains 27.26% of the overall data variance with high loadings on Na, K, Mg and a moderate loading on HCO_3. It exhibits the role of minerals weathering on chemistry of the groundwaters. The second principal component (F2) demonstrates 22.79% of the overall variance with high loadings on Fe. It highlights the role of redox processes on release of Fe^{2+} into the groundwater under the reduced conditions prevalent outside the pit. Finally, the third principal component (F3), which explains 15.75% of the overall variance corresponds to Ca, Cl, and SO_4, probably due to the dissolution of gypsum mineral and other fracture fillings of the hard-rock aquifer.

For water samples from inside the pit (group 2), F1 explains 41% of the overall data variance with negative loadings on pH and HCO_3 and moderate to high positive loadings on Eh, Cl, SO_4, Mg, SiO_2 and heavy metals (Fe and Cu). This component is certainly related to the release of elements due to the enhanced effect of AMD on weathering reactions. The second factor (F2) with high loadings on Na, K, Ca and SO_4 is probably related to dissolution of sedimentary minerals.

Biplot diagrams for the samples from outside the pit (Fig. 5A) show the main effect of the first component (F1) in water samples K1, DW3, DW4, DW6 DW14, DW10, DW13, and GD17, and the major impact of the second component (F2) on DW10, DW13, and GD17 samples. For inside the pit, biplot diagram (Fig. 5B) indicates that first factor (F1) has a positive relationship with water samples of P1, P2, P3, P4, P5, P6, and GD15, while the second component being samples P3, P7, P8, DW8, DW11, and GD15 samples.

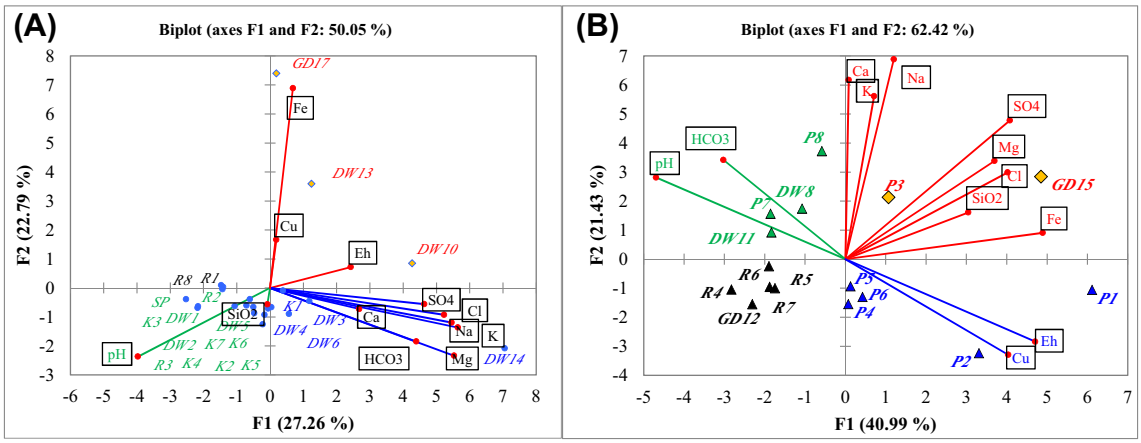

Fig. 5 Biplot diagrams for the samples from outside (**A**) and inside the pit (**B**)

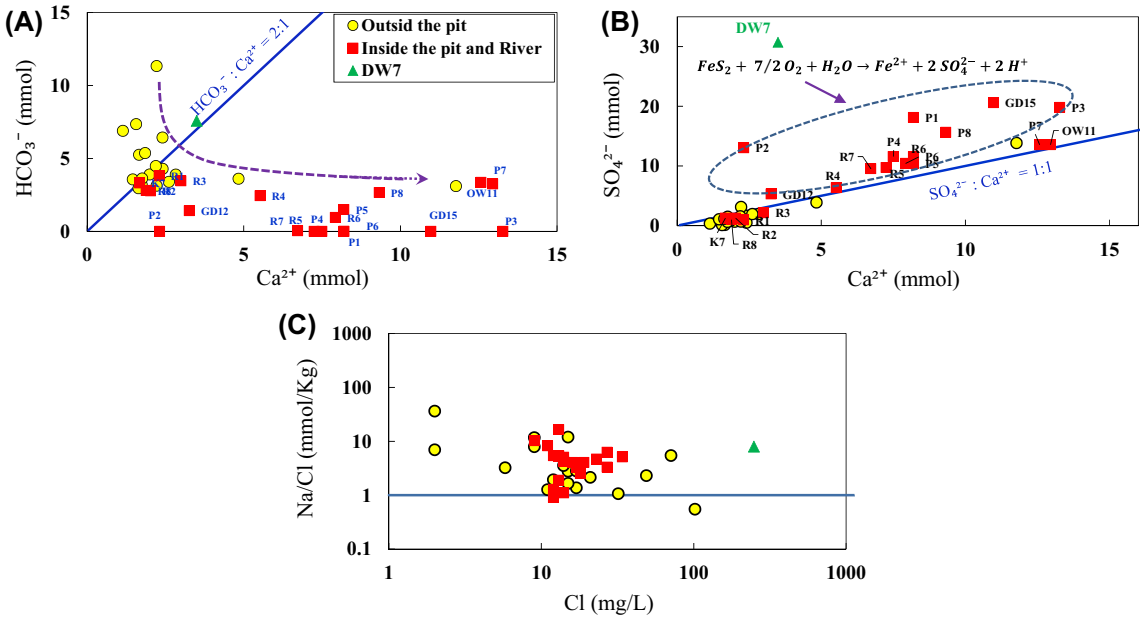

Fig.6 Composite diagrams showing HCO_3 vs. Ca (**A**), SO_4 vs. Ca (**B**) and molar ratio of Na/Cl vs. Cl (C)

Composite diagram of Ca vs. HCO_3 (Fig. 6A) clearly shows a decrease in HCO_3 concentration and an increase of the Ca towards the pit. Brackish water in the well DW7 is lying on the line 1:2, suggesting calcite dissolution as the main source of Ca and HCO_3 in this water sample. The relationship between Ca and SO_4 (Fig. 6B) shows excess SO_4 and then deviation of the pit samples from the line 1:1 of the gypsum dissolution probably due to pyrite oxidation or possibly mixing with eastern brackish waters (DW7). The molar ratio of the Na/Cl vs. Cl diagram (Fig. 6C) indicates values more than one in most samples, suggesting that in addition to halite dissolution as the main source, sodium is also derived from weathering of the Na-plagioclase (andesine).

The probable role of groundwater mixing on hydrochemical evolution of the waters inside the pit area was examined with a mixing model. The end-member-mixing-analysis (EMMA) methodology (Scheiber et al. 2018) was first used to define the number of end-members required. All of the physicochemical parameters in the water samples from inside the pit and nearby areas including EC, pH, Eh, temperature, Na, K, Ca, Mg, Cl, SO_4, HCO_3, Cu, Fe, SiO_2, $\delta^{18}O$, and δ^2H were considered for the EMMA analysis. Based on the results, two end-members and eight components (EC, Na, K, Mg, Cl, SO_4, $\delta^{18}O$, and δ^2H) are required to explain 80% of the variabilities in the chemical composition of the samples. Based on the possible hydraulic connection and chemical characteristics of the groundwater resources in Dareh-Zar mining area, two distinct fresh (Ca-HCO_3) and brackish (Na-SO_4) groundwater flows toward the pit were identified. Therefore, a mixing model considering the two end-members of fresh (sample DW5) and brackish (sample DW7) groundwaters was developed to investigate the effect of brackish water on the chemistry of the pit groundwater at a local scale, which suggested a low contribution of the brackish groundwater (on average, about 30%) to the pit water. To verify this, a plot comparing the measured and modelled value from the mixing calculations was prepared (Fig. 7). Species EC, SO_4, Mg, K, δ^2H, and $\delta^{18}O$ lie on the line 1:1, indicating that their concentrations were very dependent on mixing. For Na and Cl, however, the observed values were above the calculated values. The extremely high concentration of Na in DW7 (1284 mg/L) is 11 times greater than the Na concentration in the second most concentrated sample (DW8 = 116 mg/L). The model indicates that the mixing consists of 70%, on average, of the Ca-HCO_3 water, with presumably 30% of the Na-SO_4 water found at DW7. This seems implausible because it would take a ratio of at least 11:1 to dilute the Na concentration to that found in all the other samples. The failure of the mixing model to explain the dramatic difference in Na concentrations in most of the samples is also displayed clearly on Fig. 7, which plots estimated against observed concentrations. Only the three samples with the lowest Na concentrations (in the lower, left-hand corner of the graph), lie near the line passing through sample DW7 in the upper, right-hand corner. The same is true for the graph of estimated vs. observed Cl concentrations. The failure of the probable mixing of the fresh (Ca-HCO_3) and brackish (Na-SO_4) end-members to explain the dramatic difference of Na concentrations in most samples does not support mixing as being behind the groundwater evolution to Ca-SO_4 type water in the Dareh-Zar pit.

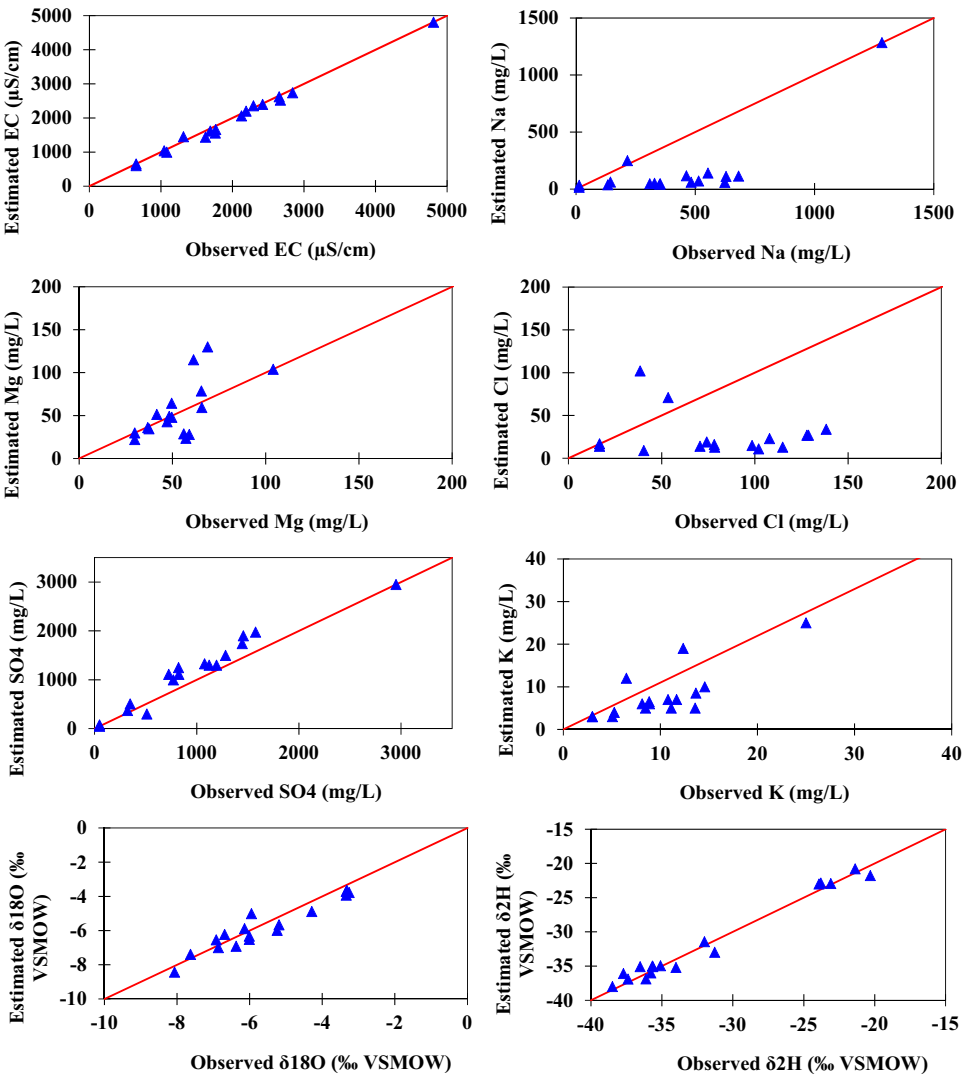

Fig. 7 Comparing the measured and calculated concentrations of species EC, SO_4, Mg, K, δ^2H, and $\delta^{18}O$ by the proposed mixing model

Therefore, it seems that the brackish waters do not affect groundwater chemistry in the pit area.

To study the chemical evolution of the mine waters in the study area, the samples were plotted on a Piper diagram (Fig. 8). Based on the results, the Ca-HCO_3 groundwater from the north and northwest areas evolve to Ca-SO_4 water-type in the pit due to pyrite oxidation. This evolutionary sequence explains the chemical composition of the groundwater samples in the Dareh-Zar mining pit.

The chemical evolution of the mine groundwater was confirmed by calculating the saturation indices (SI) of different minerals (Fig. 9). All of the samples were undersaturated with respect to halite, gypsum, pyrite and chalcopyrite (negative SI), representing their dissolution potential in mine waters. Equilibrium-to-super-saturation states ($SI \geq 0$) with respect to carbonate minerals are observed in the groundwaters outside of the pit, changing to undersaturation inside the pit area due to pyrite oxidation (Fig. 9). The process that releases sulphate into the groundwaters enhances SI values with respect to gypsum in these water samples. The groundwater samples are undersaturated with respect to copper-bearing minerals, except in the mine pit seeps where high concentrations of Cu cause the groundwater to be supersaturated and Cu minerals such as azurite and malachite to precipitate. This causes the blue-greenish colour of the seepages in the pit (Fig. 2B).

Pyrite is the dominant sulphide mineral in almost all geological environments, especially metal ore and coal deposits. It is stable under reducing conditions and oxidizes when exposed to oxygen (Rimstidt and Vaughan 2003). The acid generated by pyrite oxidation in turn speeds up the leaching of trace elements, which explains the negative relationship of pH with major ions (except for HCO_3) and trace elements (Table 4). The significant positive correlation of Fe-SO_4 ($R = 0.98$) and negative correlation of pH-Fe ($R = -0.91$) and pH-SO_4 ($R = -0.87$) confirm the importance of pyrite oxidation in the Dareh-Zar pit and explains why Cu is supersaturated in seepage waters inside the pit.

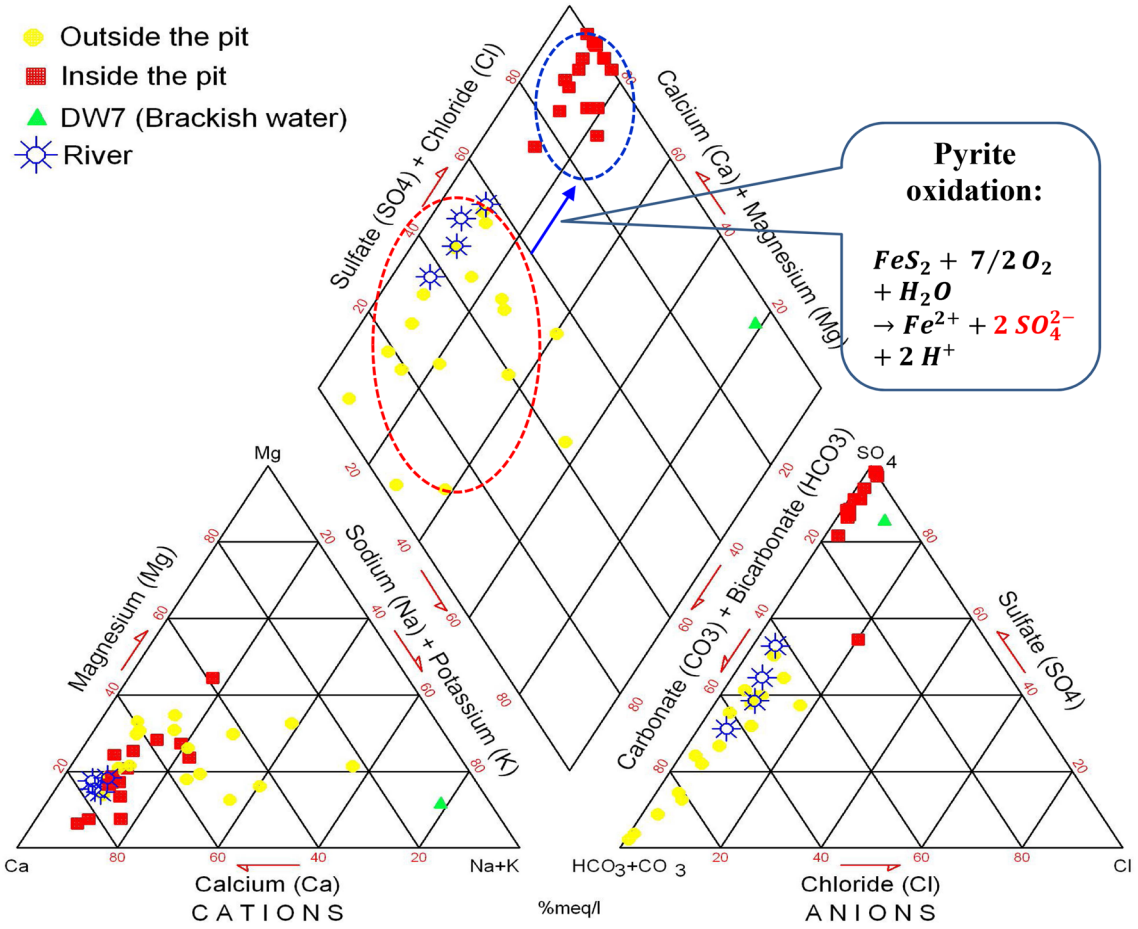

Fig. 8 Hydrochemical evolution of the groundwaters in Dareh-Zar mining area

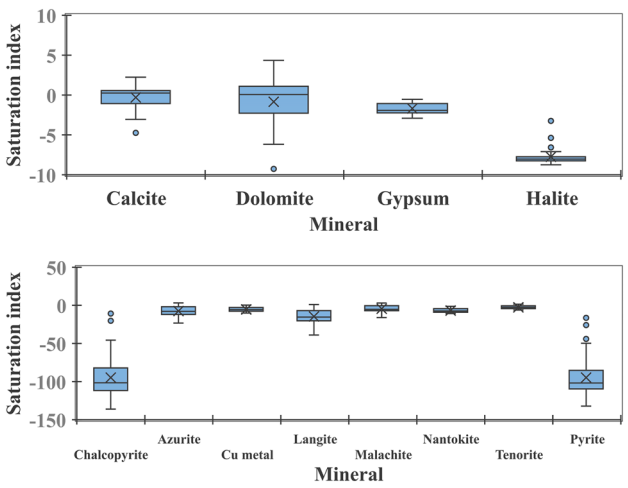

Fig. 9 Box plots representing saturation indices with respect to calcite, dolomite, gypsum, halite, Cu-bearing minerals and pyrite

The Stable Isotopes (^{18}O and ^{2}H) of the Mine Water

The $\delta^{18}O$ and $\delta^{2}H$ values in the groundwater samples (Table 1) ranged from − 8.07 to − 3.26‰ and − 38.49 to − 22.31‰, respectively, with average values of − 5.38 and − 30.39‰. Compared with the isotopic content of the local precipitation (Fig. 10A), mine waters from the Dareh-Zare area plotted on the right side of the local meteoric water line (LMWL), $\delta^{2}H = 7.22$ and $\delta^{18}O + 15.22$ (Sahraei Parizi and Samani 2014), lying mostly on the evaporation line of the region ($\delta^{2}H = 4.22$ and $\delta^{18}O$-14.85). The isotopic contents are the same as the groundwater from the Sarcheshmeh copper mine (Sahraei Parizi and Samani 2014), suggesting a similar origin for the groundwater. Higher enrichment of the isotopes due to evaporation was observed in the Darh-Zare mining area. Greater enrichments were observed in the seeps and mine waters sampled from the pit, suggesting that evaporation affected the isotopic and chemical composition of the groundwater. The isotopes in the Dareh-Zare mine groundwater were also similar to the isotopic content of the

Table 4 Pearson's correlation coefficients between pH and SO_4 with other chemical parameters in water samples from inside the pit of Dareh-Zar mine. Values in bold letters show significant correlations

	Na	K	Ca	Mg	Cl	SO_4	HCO_3	SiO_2	Fe	Cu
pH	− 0.36	0.01	0.46	**− 0.94**	**− 0.67**	**− 0.87**	0.45	**− 0.54**	**− 0.91**	**− 0.99**
SO_4	0.70	− 0.32	0.02	**0.92**	**0.82**	**1**	− 0.46	**0.85**	**0.98**	**0.87**

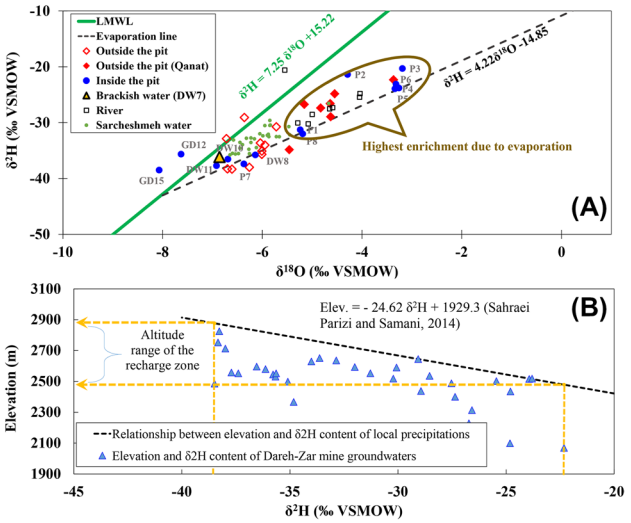

Fig. 10 The composition of stable isotopes ($\delta^{18}O$ and $\delta^{2}H$) in groundwater resources of Dareh-Zar mine as compared with local meteoric water line (LMWL), the evaporation line of the region (Sahraei Parizi and Samani 2014) and water samples from Sarcheshmeh mine (**A**) and the approximate elevation of the recharge zone of the Dareh-Zar (**B**) based on the elevation-$\delta^{2}H$ relationship in local precipitation

surface waters (river samples) and qanats, all showing major evaporative effects.

The approximate elevation of the recharge zone of the Dareh-Zare mine was calculated based on the relationship between elevation and isotopic contents of the local precipitation (elevation = − 24.62$\delta^{2}H$ + 1929.3; Sahraei Parizi and Samani 2014; Fig. 10B). Considering no isotopic enrichments of recharge in the vadose zone and groundwater aquifer, the minimum and maximum elevations of the recharge zone of Dareh-Zare mine were calculated to be at 2479 and 2877 m a.m.s.l, respectively.

The final groundwater model of Dareh-Zar copper mine was determined (Fig. 11) based on hydraulic features inferred from the iso-potential map of the aquifer and analysis of the chemo-isotopic data, and the major role of fresh (Ca-HCO_3) groundwaters on chemistry of the mine pit groundwaters was recognised. It confirmed the main origin of the pit water from the north and northwestern parts of the mining area through permeable zones and faults, as shown in the proposed conceptual model (Fig. 11). Based on the drilling logs of the exploration wells, a weathered-fractured permeable zone at altitude of 2500 to 2600 m a.m.s.l. exists in the study area (Mali et al. 2021), which exactly coincides with the mean altitude of the seepage faces inside the mine pit. This agrees with the elevation of the recharge zone calculated by the isotopes (2479 and 2877 m a.m.s.l.), proving the role of this permeable zone in transferring groundwater into the Dareh-Zar mining pit. The Ca-HCO_3 groundwaters form the north and northwest areas evolve along the groundwater flow paths and change to Ca-SO_4 water-type in the mining pit due to pyrite oxidation. This suggests that the groundwater originates from these northern and northwestern recharge zones.

Conclusion

In the Dareh-Zar copper mine study area, the groundwater generally flows from the northwest to the southeast. This groundwater is being discharged by seepage faces in the Dareh-Zar mine pit, springs, and qanats. Because of excavation and related dewatering process, groundwater incursions have occurred in the mine pit, leading to the formation of many seepage faces with AMD features. Hence, problems such as flooding, pit wall instability, and AMD are expected in the future. The chemistry and isotopic characteristics of the groundwaters from outside and inside the pit were investigated to determine the origin of the seepage water in the pit. PCA and biplot diagrams showed that the major factors controlling the groundwater chemistry outside the pit were mineral weathering, redox reactions (causing the release of Fe), and gypsum dissolution, while the formation of AMD and dissolution of sedimentary minerals were the key reactions inside the pit. Composite diagrams displayed dissolution of calcite, gypsum, and halite minerals as the main reactions changing the chemistry of the groundwater. AMD production due to pyrite oxidation changes the equilibrium states of carbonate minerals and dissolution of copper-bearing minerals, except in areas in the mine pit where high concentrations of Cu cause the groundwater to be supersaturated and Cu minerals such as azurite and malachite to precipitate.

Ca-HCO_3 (fresh) and Na-SO_4 (brackish) groundwaters were identified northwest and east of the mine, respectively, changing to Ca-SO_4 inside the mining pit. Examination of a probable mixing model considering the fresh and brackish end-members showed that the brackish water has no effect

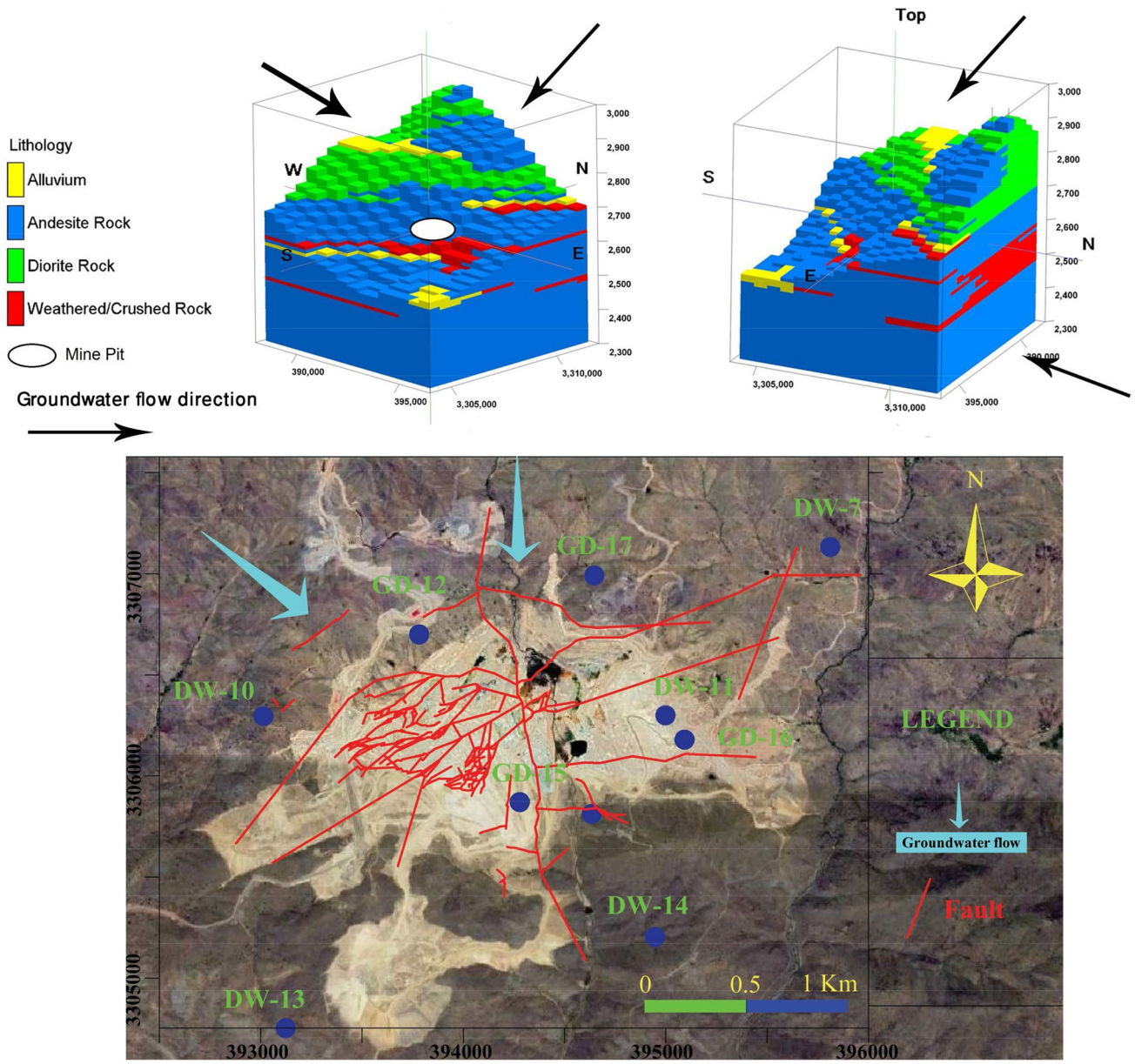

Fig. 11 The hydrogeological conceptual and groundwater flow model of the Dareh-Zar copper mine, which explains the source and chemical evolution of groundwater resources

on pit groundwater and that pyrite oxidation is responsible for the final composition of the pit groundwater being the Ca-SO_4 water type. In other words, the Ca-HCO_3 groundwater from north and northwest of the mine evolves to Ca-SO_4 water-type in the pit due to pyrite oxidation. Pearson's correlation coefficients between pH and SO_4 with other chemical parameters confirmed the importance of pyrite oxidation in the release of metals into the groundwater as it speeds up the leaching of trace elements and explains why copper is supersaturated in the pit's seeps.

According to the stable isotopes $\delta^{18}O$ and $\delta^{2}H$, the mine waters from the Dareh-Zar area mostly plotted on the evaporation line of the region, right of the LMWL indicating enrichment of the isotopes due to evaporation. The relationship between elevation and $\delta^{2}H$ showed more depletion in isotopic contents at higher elevations. The stable isotopes confirmed the origin of the pit groundwater from local precipitation, and that it is being recharged from surrounding topographic highs at elevations of 2479 to 2877 m a.m.s.l. Thus, groundwater inrushes to the

Dareh-Zar pit area is probably from the north and northwest recharge zones. These areas need special attention as a mine drainage system is designed to control groundwater inrush into the mine area and prevent subsequent related operational, technical, and environmental disasters.

Acknowledgements The authors thank the National Iranian Copper Industry Co. and Dr. H. Sahraei Parizi.

References

Ahmadi S, Jahanshahi R, Moeini V, Mali S (2018) Assessment of hydrochemistry and heavy metals pollution in the groundwater of Ardestan mineral exploration area. Iran Environ Earth Sci 77:212

Alegbe MJ, Ayanda OS, Ndungu P, Nechaev A, Petrik LF (2019) Physicochemical characteristics of acid mine drainage, simultaneous remediation and use as feedstock for value added products. J Environ Chem Eng 7(3):103097

Amajor LC, Gbadebo AM (1992) Oil field brines of meteoric and connate origin in the eastern Niger delta. J Pet Geol 15(4):481–488

Askari Malekabad F, Jahanshahi R, Bagheri R (2020) Characterization of the Bazman geothermal field, the southeast of Iran. Geopersia 10(2):405–418

Bahadori D, Jahanshahi R, Dehghani V, Mali S (2019) Variations of stable oxygen and hydrogen isotope ratios in the cold and thermal springs of the Bazman volcanic area (in the southeast of Iran). Environ Earth Sci 78:663

Cao X, Zhou S, Xie F, Rong R, Wu P (2019) The distribution of rare earth elements and sources in Maoshitou reservoir affected by acid mine drainage, southwest China. J Geochem Explor 202:92–99

Carrera J, Vázquez-Suñé E, Castillo O, Sánchez-Vila X (2004) A methodology to compute mixing ratios with uncertain endmembers. Water Resour Res 40:W12101

Christensen JN, Dafflon B, Shiel AE, Tokunaga TK, Wan J, Faybishenko B, Dong W, Williams KH, Hobson C, Brown ST, Hubbard SS (2018) Using strontium isotopes to evaluate the spatial variation of groundwater recharge. Sci Total Environ 637–638:672–685

Clark ID, Fritz P (1997) Environmental Isotopes in Hydrogeology. Lewis Publishers, Boca Raton

Dimitrijevic MD, Dimitrijevic MN, Djordjevic M, Vulovic D (1956) Geological map of Iran 1:100000 Series, Sheet 7149-Pariz. Ministry of Economy, Geological Survey of Iran

Faye S, Maloszewski P, Stichler W, Gaye CB (2005) Groundwater salinization in the Saloum (Senegal) delta aquifer: minor elements and isotopic indicators. Sci Total Environ 343:243–259

Gamboa C, Godfrey L, Herrera C, Custodio E, Soler A (2019) The origin of solutes in groundwater in a hyper-arid environment: A chemical and multi-isotope approach in the Atacama Desert. Sci Total Environ, Chile. https://doi.org/10.1016/j.scitotenv.2019.06.356

Ghiglieri G, Carletti A, Pittalis D (2012) Analysis of salinization processes in the coastal carbonate aquifer of Porto Torres (NW Sardinia, Italy). J Hydrol 432–433:43–51

Gomo M (2018) Conceptual hydrogeochemical characteristics of a calcite and dolomite acid mine drainage neutralised circumneutral groundwater system. Water Sci 32(2):355–361

Gomo M, Vermeulen D (2014) Hydrogeochemical characteristics of a flooded underground coal mine groundwater system. J Afr Earth Sci 92:68–75

Gu H, Ma F, Guo J, Li K, Lu R (2018) Assessment of water sources and mixing of groundwater in a coastal mine: the Sanshandao gold mine, China. Mine Water Environ 37:351–365

Guan ZL, Jia ZF, Zhao ZQ, You QY (2019) Identification of inrush water recharge sources using hydrochemistry and stable isotopes: a case study of Mindong No. 1 coal mine in north-east Inner Mongolia. China. J Earth Syst Sci 128(200):2–12

Guo BH, Cheng T, Wang L (2018) Physical simulation of water inrush through the mine floor from a confined aquifer. Mine Water Environ 37:577–585

Hao C, Huang Y, He P, Sun W (2019) Isotope drift characteristics in Ordovician limestone karst water caused by coal mining in northern China. Mine Water Environ 38:507–516

Heidari–Nejad H, Zarei M, MerkelBJ k, (2017) Evaluating the origin of seepage water in the Golgohar iron mine. Iran. Mine Water Environ 36:583–596

Hu XY, Wang LG, Lu YL, Yu M (2014) Analysis of insidious fault activation and water inrush from the mining floor. J Chin Univ Min Technol 24(4):477–483

Hu Y, Li W, Wang Q, Liu S, Wang Z (2019a) Evolution of floor water inrush from a structural fractured zone with confined water. Mine Water Environ 38:252–260

Hu Y, Sun J, Liu W, Wei D (2019b) The evolution and prevention of water inrush due to fault activation at working face no. II 632 in the Hengyuan coal mine. Mine Water Environ 38:93–103

Huang PH, Yang ZY, Wang XY, Ding FF (2019) Research on Piper PCA-Bayes-LOOCV discrimination model of water inrush source in mines. Arab J Geosci 12:334

Huang X, Wang GC, Liang XY, Cui LF, Ma L, Xu QY (2018) Hydrochemical and stable isotope (δD and δ18O) characteristics of groundwater and hydrogeochemical processes in the Ningtiaota coalfield, northwest China. Mine Water Environ 37(1):119–136

Jahanshahi R, Zare M (2015) Assessment of heavy metals pollution in groundwater of Golgohar iron ore mine area. Iran Environ Earth Sci 74:505–520

Jahanshahi R, Zare M (2017) Delineating the origin of groundwater in the Golgohar mine area of Iran using stable isotopes of 2H and 18O and hydrochemistry. Mine Water Environ 36(4):550–563

Jamal A, Dhar BB, Ratan S (1991) Acid mine drainage control in an opencast coal mine. Mine Water Environ 10(1):1–16

Jin Z, Zheng Q, Zhu C, Wang Y, Cen JR, Li FL (2018) Contribution of nitrate sources in surface water in multiple land use areas by combining isotopes and a Bayesian isotope mixing model. Appl Geochem 93:10–19

Jurado A, Vàzquez-Suñé E, Soler A, Tubau I, Carrera J, Pujades E, Anson I (2013) Application of multi-isotope data (O, D, C and S) to quantify redox processes in urban groundwater. Appl Geochem 34:114–125

Karolytė R, Johnson G, Serno S, Gilfillan SMV (2017) The influence of water-rock reactions and O isotope exchange with CO_2 on water stable isotope composition of CO_2 springs in SE Australia. Energy Procedia 114:3832–3839

Khorasanipour M, Eslami A (2014) Hydrogeochemistry and contamination of trace elements in Cu-porphyry mine tailings: a case study from the Sarcheshmeh Mine, SE Iran. Mine Water Environ 33:335–352

Larkins C, Turunen K, Mänttäri I, Lahaye Y, Hendriksson N, Forsman P, Backnäs S (2018) Characterization of selected conservative and non-conservative isotopes in mine effluent and impacted surface waters: implications for tracer applications at the mine-site scale. Appl Geochem 91:1–13

Lee D, Yim G-J, Ji S-W, Cheong Y-W (2013) Study on distribution characteristics of some water parameters properties of mine drainage in an oxidation pond, Hwangji-Yuchang coal mine, South Korea. Environ Earth Sci 68:241–249

Lenter CM, McDonald LM, Skousen JG, Ziemkiewicz PF (2002) The effects of sulfate on the physical and chemical properties of actively treated acid mine drainage floc. Mine Water Environ 21(3):114–120

Li B (2019) Wu Q (2019) Catastrophic evolution of water inrush from a water-rich fault in front of roadway development: a case study of the Hongcai coal mine. Mine Water Environ 38:421–430

Li P, Tian R, Liu R (2019) Solute geochemistry and multivariate analysis of water quality in the Guohua phosphorite mine, Guizhou Province. China Expo Health 11(2):81–94

Li P, Wu J, Qian H (2016) Preliminary assessment of hydraulic connectivity between river water and shallow groundwater and estimation of their transfer rate during dry season in the Shidi River. China Environ Earth Sci 75(2):99

Li P, Wu J, Tian R, He S, He X, Xue C (2018) Zhang K (2018) Geochemistry, hydraulic connectivity and quality appraisal of multilayered groundwater in the Hongdunzi Coal Mine, northwest China. Mine Water Environ 37:222–237

Liu JT, Yj H, Gao ZJ, Wang M, Liu MX, Wang ZY, Wang S (2019) Determining the factors controlling the chemical composition of groundwater using multivariate statistics and geochemical methods in the Xiqu coal mine, north China. Environ Earth Sci 78:364

Ma L, Qian JZ, Zhao WD, Curtis Z, Zhang RG (2016) Hydrogeochemical analysis of multiple aquifers in a coal mine based on non-linear PCA and GIS. Environ Earth Sci 75(8):1–14

Ma R, Shi JS, Liu JC, Gui CL (2014) Combined use of multivariate statistical analysis and hydrochemical analysis for groundwater quality evolution: a case study in North China Plain. J Earth Sci 25(3):587–597

Mali S, Jafari H, Jahanshahi R (2021) Identifying the permeable zones in Dare-h-Zar copper mining area in Sirjan using time series analysis of the precipitation and groundwater level. Hydrogeology 5(2):127–141 ((**in Persian**))

Mondal NC, Singh VS, Saxena VK, Singh VP (2011) Assessment of seawater impact using major hydrochemical ions: a case study from Sadras, Tamilnadu, India. Environ Monit Assess 177:315–335

Naderi M, Jahanshahi R, Dehbandi R (2020) Two distinct mechanisms of fluoride enrichment and associated health risk in springs' water near an inactive volcano, southeast Iran. Ecotoxicol Environ Saf 195:110503

Parkhurst DL, Appelo C (1999) User's Guide to PHREEQC (Version 2): A Computer Program for Speciation, Batch-Reaction, One-Dimensional Transport, and Inverse Geochemical Calculations Water-Resources. USGS Investigations Report 99–4259

Pitkänen P, Löfman J, Koskinen L, Leino-Forsman H, Snellman M (1999) Application of mass-balance and flow simulation calculations to interpretation of mixing at Äspö. Sweden Appl Geochem 14(7):893–905

Pyrbot W, Shabong L, Singh O (2019) Neutralization of acid mine drainage contaminated water and ecorestoration of stream in a coal mining area of east Jaintia Hills, Meghalaya. Mine Water Environ 38:551–555

Qian J, Tong Y, Ma L, Zhao W, Zhang R, He X (2018) Hydrochemical characteristics and groundwater source identification of a multiple aquifer system in a coal mine. Mine Water Environ 37:528–540

Qian JZ, Wang L, Ma L, Lu YH, Zhao WD, Zhang Y (2016) Multivariate statistical analysis of water chemistry in evaluating groundwater geochemical evolution and aquifer connectivity near a large coal mine, Anhui. China Environ Earth Sci 75(9):3–10

Rambabu S, Venkatesh AS, Syed TH, Surinaidu L, Srinivas P, Rai SP, Manoj K (2018) Stable isotope systematics and geochemical signatures constraining groundwater hydraulics in the mining environment of the Korba coalfield, central India. Environ Earth Sci 77(15):2–17

Rimstidt JD, Vaughan DJ (2003) Pyrite oxidation: a state-of-the-art assessment of the reaction mechanism. Geochim Cosmochim Acta 67:873–880

Sahraei Parizi H, Samani N (2014) Environmental isotope investigation of groundwater in the Sarcheshmeh copper mine area. Iran Mine Water Environ 33:97–109

Sahraei Parizi H, Samani N (2013) Geochemical evolution and quality assessment of water resources in the Sarcheshmeh copper mine area (Iran) using multivariate statistical techniques. Environ Earth Sci 69:1699–1718

Scheiber L, Ayora C, Vázquez-Suñé E (2018) Quantification of proportions of different water sources in a mining operation. Sci Total Enviro 619–620:587–599

Shojaei Baghini S, Jahanshahi R, Mali S, Nasiri MA (2020) Destruction of groundwater quality and the risk of saltwater intrusion in the aquifers nearby Sirjan salt playa. Iran Int J Environ Anal Chem 100(6):647–661

Shrestha S, Kazama F (2007) Assessment of surface water quality using multivariate statistical techniques: a case study of the Fuji River basin. Japan Environ Model Softw 22(4):464–475

Skousen JG, Ziemkiewicz PF, McDonald LM (2019) Acid mine drainage formation, control and treatment: approaches and strategies. Extr Ind Soc 6(1):241–249

Sprenger C, Parimala Renganayaki S, Schneider M, Elango L (2014) Hydrochemistry and stable isotopes during salinity ingress and refreshment in surface- and groundwater from the Arani-Koratallai (A–K) basin north of Chennai (India). Environ Earth Sci 73:7769–7780

Struzina M, Müller M, Drebenstedt C, Mansel H, Jolas P (2011) Dewatering of multi-aquifer unconsolidated rock opencast mines: alternative solutions with horizontal wells. Mine Water Environ 30:90–104

Tomiyama S, Igarashi T, Tabelin C, Tangviroon P, Ii H (2019) Acid mine drainage sources and hydrogeochemistry at the Yatani mine, Yamagata, Japan: a geochemical and isotopic study. J Contam Hydrol 225:103502

Tomonaga Y, Marzocchi R, Pera S, Pfeifer HR, Kipfer R, Decrouy L, Vennemann T (2016) Using noble–gas and stable–isotope data to determine groundwater origin and flow regimes: application to the Ceneri Base Tunnel (Switzerland). J Hydrol 545:395–409

Williams H, Turner FJ, Gilbert CM (1982) Petrography. An Introduction to the Study of Rocks in Thin Sections, Freeman and Company, New York City

Wu J, Li P, Qian H, Duan Z, Zhang X (2014) Using correlation and multivariate statistical analysis to identify hydrogeochemical processes affecting the major ion chemistry of waters: case study in Laoheba phosphorite mine in Sichuan. China Arab J Geosci 7(10):3973–3982

Wu Q, Liu Y, Wu X, Liu S, Sun W, Zeng Y (2016) Assessment of groundwater inrush from underlying aquifers in Tunbai coal mine, Shanxi province. China Environ Earth Sci 75:737

Wunderlin DA, Diaz MP, Ame MV, Pesce SF, Hued AC, Bistoni MA (2001) Pattern recognition techniques for the evaluation of spatial and temporal variations in water quality. A case study: suquia River basin (Cordoba, Argentina). Water Res 35(12):2881–2894

Xu Z, Sun Y, Gao S, Zhao X, Duan R, Yao M, Liu Q (2018) Groundwater source discrimination and proportion determination of mine inflow using ion analyses: a case study from the Longmen coal mine, Henan Province, China. Mine Water Environ 37:385–392

Yang J, Dong S, Wang H, Li G, Wang T, Wang Q (2021) Mine water source discrimination based on hydrogeochemical characteristics in the northern Ordos Basin, China. Mine Water Environ 40:433–441

Yang Z, Huang P, Ding F (2020) Groundwater hydrogeochemical mechanisms and the connectivity of multilayer aquifers in a coal mining region. Mine Water Environ 39:808–822

Yidana SM, Yidana A (2010) An assessment of the origin and variation of groundwater salinity in southeastern Ghana. Environ Earth Sci 61:1259–1273

Yolcubal I, Demiray AD, Çiftçi E (2017) Assessment of acid mine drainage potential of flotation slurry from a tailing dam in a copper mine, Murgul, northeastern Turkey. Environ Earth Sci 76:100

Zhang H, Xu G, Chen X, Mabaire A, Zhou J, Zhang Y, Zhang G, Zhu L (2020) Groundwater hydrogeochemical processes and the connectivity of multilayer aquifers in a coal mine with karst collapse columns. Mine Water Environ 39:356–368

Zhang H (2020) Yao D (2020) The Bayes recognition model for mine water inrush source based on multiple logistic regression analysis. Mine Water Environ 39:888–901

Zhao J, Fu G, Lei K, Li YW (2011) Multivariate analysis of surface water quality in the three gorges area of China and implications for water management. J Environ Sci 23(9):1460–1471

Zhao Y, Li PF, Tian SM (2013) Prevention and treatment technologies of railway tunnel water inrush and mud gushing in China. J Rock Mech Geotech Eng 5(6):468–477

Zhou J, Zhang Q, Kang F, Zhang Y, Yuan L, Wei D, Lin S (2018a) Using multi-isotopes (34S, 18O, 2H) to track local contamination of the groundwater from Hongshan-Zhaili abandoned coal mine, Zibo city, Shandong province. Int Biodeterior Biodegr 128:48–55

Zhou QL, Juan H, Arturo H (2018b) The numerical analysis of fault-induced mine water inrush using the extended finite element method and fracture mechanics. Mine Water Environ 37:185–195